J MATER RES TECHNOL. 2020;9(5):11861–11875

Available online at www.sciencedirect.com

jmr&t Journal of Materials Research and Technology

https://www.journals.elsevier.com/journal-of-materials-research-and-technology

Original Article

High performance graphene-based PVF foam for lead removal from water

Mohammed Yosef[a], *Alaa Fahmy*[a,b], *Walid El Hotaby*[c], *Ali M. Hassan*[a], *Ahmed S.G. Khalil*[d,e], *Badawi Anis*[c,*]

[a] *Chemistry Department, Faculty of Science, Al-Azhar University, 11884 Cairo, Egypt*
[b] *BAM Federal Institute for Materials Research and Testing, Unter den Eichen 87, 12205 Berlin, Germany*
[c] *Spectroscopy Department, Physics Division, National Research Centre, 33 El Bohouth st., Dokki, Giza P.O. 12622, Egypt*
[d] *Materials Science & Engineering Department, School of Innovative Design Engineering, Egypt-Japan University of Science and Technology (E-JUST), P. O. Box 179 New Borg El-Arab City, Alexandria, Egypt*
[e] *Physics Department and Center for Environmental and Smart Technology, Faculty of Science, Fayoum University, 63514 Fayoum, Egypt*

ARTICLE INFO

Article history:
Received 11 May 2020
Accepted 2 August 2020

Keywords:
Graphene oxide
Lead ions
Polyvinyl formaldehyde foam
Superior sorbent
Water treatment

ABSTRACT

The synthesis and optimization of superior and eco-friendly sorbents for Pb(II) pose a great challenge in the field of water treatment. The sorbent was developed by introducing graphene oxide (GO) into the matrix of polyvinyl formaldehyde (PVF) foam. The immobilization of GO in PVF results in significant increase in the maximum adsorption capacity (Qt) of GO powder for Pb(II), from ≈800 to ≈1730 mg g^{-1} in the case of GO/PVF foam. As compared with GO powder in Pb(II) aqueous solutions, PVF matrix keeps GO sheets stable without any agglomeration. The large surface area of GO sheet allows the abundant oxygenated functional groups on its surface to participate effectively in the Pb(II) adsorption process, leading to the huge increase of the Qt. Adsorption isotherms and kinetic studies indicated that the sorption process of Pb(II) on GO/PVF was done on heterogenous surface by ion-exchange reaction. The GO/PVF foam showed an excellent reusability for more than 10 cycles with almost the same efficiency and without any significant change in its physical properties.

1. Introduction

Discharging of Pb(II) is considered as one of the main persistent pollutant for aquatic environments [1,2]. The presence of even minor concentrations of Pb(II) in water can cause great threat to humans and ecosystems [3]. Nowadays, several traditional methods including nano-filtration, ion-exchange, precipitation, reverse osmosis, coagulation, and adsorption are used for Pb(II) removal from wastewater [4–6]. In particular, adsorption is more favorable over other traditional methods due to its high removal capacity, flexibility in design, ease of operation, and relatively low cost [7].

Several ligand based composite materials have been used as efficient detecting and absorbing sorbents for Pb(II) and other toxic materials from water [8–11]. Recently, carbon nanotubes (CNTs), graphene, and graphene oxide (GO) have emerged as an efficient organic and inorganic pollutants

* *Corresponding author.*
E-mails: alaa.fahmy@azhar.edu.eg (A. Fahmy), badawi.ali@daad-alumni.de (B. Anis).
https://doi.org/10.1016/j.jmrt.2020.08.011

adsorbents [12,13]. Among them, GO has received more attention in heavy metal ions removal due its great mechanical properties, relatively large surface area, chemical stability, and presence of plenty of oxygenated functional groups [14,15].

Several GO nanocomposites have been widely used in the removal of Pb(II) from aqueous solutions [16]. Graphene oxide and GO-montmorillonite nanocomposite have shown a maximum adsorption capacity of 20 and 19.79 mg g^{-1}, respectively [17]. Deng et al. demonstrated that the adsorption capacity of hexafluorophosphate functionalized graphene (GNS^{PF6}) reached 400 mg g^{-1} [18]. The adsorption capacity of GO has been enhanced by activating GO surface using EDTA-silane. The adsorption capacity of the prepared EDTA-GO reached ≈479 mg g^{-1} [19]. Modified GO with manganese ferrite magnetic nanoparticles, GO-$MnFe_2O_4$, showed adsorption capacity of 673 mg g^{-1} for Pb(II) within 10 min [20]. Highly oxidized GO showed an impressive maximum adsorption capacity of 842 mg g^{-1} [21], 931.66 mg g^{-1} [14], and 1119 mg g^{-1} [22]. In addition, GO has been used as high performance phosphate removal [23], organic surfactant removal [24,25], removal of dyes [26], and recovery of nobel metals [27]. Therefore, the high adsorption capacity, cost effective, and antibacterial nature proposed GO as a superior candidate for the production of water treatment systems. However, the direct use of GO or modified GO powder in water treatment has some environmental and health concerns as it could be a source of water contaminations [28]. Due to its superhydrophilicity and high water dispersibility, the separation process of GO is difficult and further advanced techniques such as filtration and centrifugation are needed. These difficulties limit the usage of GO powder as a practical sorbent in the production of safe water.

Formation of GO 3D macrostructures could be a versatile solution to overcome the challenges mentioned above. The 3D macrostructure provides large surface area and well interconnected porous providing ample of oxygenated functional groups available for metal adsorption [29]. Several works have constructed and designed several 3D graphene and GO based adsorbents. These retain the fascinating properties of the graphene based materials in addition to new physiochemical properties such as low density, high porosity, and large surface area [30]. Recently several 3D porous architecture based on GO composites have been prepared for Pb(II) removal such as 3D GO/starch architecture [31], 3D hierarchical GO/xanthan/TiO_2 [32], GO/chitosan aerogels [33], magnetic GO beads [34], Polydopamine/GO Hydrogel [35], and polysiloxane/GO Sponge [36]. All the above mentioned 3D structures have shown adsorption capacity in the range of ≈108–373 mg g^{-1} for Pb(II). In addition to Pb(II) removal, 3D GO composites have been used in removing rare earth elements [37–39]. Despite enhancing the adsorption capacity and solving the environmental concerns, the preparation of the 3D GO architectures is still very costly, since very expensive and sophisticated techniques are used. These difficulties hinder their implementation as a practical sorbents. To tackle this need, immobilization of GO sheets onto large surface of low cost 3D polymeric materials can solve the above technical issues. Recently, Feng et al. [40], immobilized GO onto commercially low cost melamine sponge using polydopamine as a linker between the sponge surface and GO sheets. The main disadvantage of GO/melamine sponge is that after five cycles of reuse the adsorption capacity was greatly reduced from 349.7 to ≈175 mg g^{-1}, this could be due releasing of some bounded GO sheets from the surface of the melamine sponge.

Composites obtained from biocompatible polymers, such as polyvinyl alcohol (PVA), are more preferable over other synthetic and natural source [41]. PVF foams are well-known spongy materials which are widely used in many domestic and medical applications due to their great advantages such as; ease of production, low cost, high water absorption capacity, good mechanical properties, and biocompatibility [42].

Here, we report the immobilization of GO sheets onto polyvinyl-formaldehyde (PVF) foam matrix. Super-hydrophilic GO powder was homogenously distributed in water using tip-sonication, then GO was incorporated into a PVF foam matrix during the foaming process. The possible interactions between the Pb(II) and the surface of GO sheets in the powder form and in comparison to that immobilized onto PVF foam were studied. Kinetic and isotherm experiments were performed to analyze the removal efficiency and sorption mechanisms of Pb(II) using the developed GO/PVF foam.

The using of GO/PVF foam as sorbent for heavy metal suggests facile and efficient recovery method, escaping the traditional recovery pathways such as filtration, centrifugation, magnetic separation, and precipitation by pH shift. In real applications, these methods appear as unsuitable for treatment of large quantity of wastewater; involving time/energy consuming and complicated steps. Therefore, the sponge-like structure GO/PVF is postulated here to enable the sorbent isolation from water, just by hand-capturing. The proposed sorbent may be used in fixed-bed reactors under the flow of wastewater. Hence, the recovery of the sorbent from the liquid medium is incorporated into the method used for its preparation. The GO/PVF will address the sustainability criteria, including those related to environmental, economic and remediation issues.

2. Experimental

2.1. Materials

Dry flakes of expandable graphite (3772, 300 μm nominal size, Asbury Carbons, USA) was used. High molecular weight and fully hydrolyzed polyvinyl alcohol (PVA, 98–99%, degree of polymerization 1700–1800), was purchased from LOBA Chemie. Lead nitrate (analytical grade) and potassium permanganate ($KMnO_4$) were purchased from Merck. Triton X-100 was purchased from Sigma Aldrich. Formaldehyde, hydrogen peroxide (H_2O_2, 35%), hydrochloric acid (HCl, 37%), sulphuric acid (H_2SO_4, 98%), and hypophosphoric acid (H_3PO_4, 85%) were obtained from Fisher. Milli-Q water was used in all experiments.

2.2. Preparation of graphene oxide

Monolayers of highly oxidized GO was prepared using improved Hummers' method [43,44]. Briefly, the dry expandable graphite flakes were heated at 1050 °C for 30 s. Thermally

expanded graphite (3 g) was then added to a 400 mL of H_2SO_4:H_3PO_4 (9:1 mL) mixture. $KMnO_4$ (18 g) was added very slowly to the mixture placed in ice-bath. The mixture was stirred at 50 °C for ≈2 h and the stirring continued for 3 days at room temperature. The graphite/acids solution turned light brown paste-like mixture. The graphite paste was added slowly in aliquot to an ice mixture of deionized water H_2O_2 (400 mL) and 5 mL of 30% H_2O_2. A bright golden GO solution was formed. The GO solution was filtered and washed with 10 wt% HCl solution several times then with water until the pH reached nearly 5 [45]. The precipitate was dried under vacuum at 60 °C for 6 h.

2.3. Preparation of GO/PVF foams

The PVF foam was prepared as follows: 10 mL of formaldehyde was added to 10 wt% PVA hot solution (60 g) under stirring for 5 min. Then, 1 mL of Triton X-100 was added, and stirring was continued for 10 min. The PVA formaldehyde solution was cooled down to ≈25 °C then 30 mL H_2SO_4 (15 wt%) was added with stirring for 15 min. Then the solution was baked at 60 °C for 5 h. To remove unreacted formaldehyde and Triton from the formed PVF foam, the foam was washed with hot water several times and dried at 60 °C under vacuum overnight [46,47]. The prepared PVF foam has a white color and is cylindrical in shape as shown in Fig. 1(a).

The GO/PVF foam was prepared as follows:, 200 mg of GO powder was ultra-sonicated for 2 h in an ice-bath-cooled water (30 mL). The un-exfoliated GO bundles was removed by centrifugation for 1 h at 5000 rpm. The GO solution was mixed with 10 wt% hot PVA solution (60 g) by vigorous stirring for 15 min. The foaming process of GO/PVF foam completed by adding formaldehyde (10 mL), Triton X-100 (1 mL), and 30 mL H_2SO_4 (15 wt%). Then the solution was baked at 60 °C for 5 h. The color of the GO/PVF foam changed from white to homogenous brown, indicating the homogenous distribution of GO inside the PVF matrix (Fig. 1(b)). For adsorption experiment, the GO/PVF was divided into small pieces and washed again several times with water to remove any residuals of Triton X-100 and formaldehyde, which may be still present in the PVF foam. Then the GO/PVF foam pieces was dried at 60 °C for 2 h and weighted before being used in adsorption experiments, seen in Fig. 1(c) and (d).

2.4. Materials and characterizations

Transmission electron microscopy (TEM Jeol-JEM-101, Japan) was used to characterize the structural properties of GO sheets. Scanning electron microscope equipped with EDS detector (SEM, ZEISS Sigma 500 VP, Germany) was used to characterize the GO based PVA foams. Raman spectra were excited by 532 nm excitation wavelength using WITec alpha 300 R Raman-scope, Germany. Reflectance spectra were collected at ambient conditions in the frequency range 4000–400 cm^{-1} by a PLATINUM attenuated total reflection (ATR) unit attached to a Bruker vertex 80V-FTIR spectrometer, Germany. Dynamic light scattering (DLS) results were recorded by a Malvern zetasizer, United Kingdom.

2.5. Adsoprtion experiments

Firstly, a 1000 ppm Pb(II) stock solution was prepared by dissolving 1000 mg of lead nitrate in 1000 mL of water. To obtain the desired concentrations of Pb(II), the stock solution was diluted during experiments with deionized water. For studying the effect of pH, 0.05 g of dry GO/PVF foam and 25 mL of 150 ppm Pb(II) solution were used. The pH value was changed from 3 to 8 by adding few drops of 0.1 M NaOH or 0.1 M HCl with stirring. Different weights of GO/PVF foam: 0.05, 0.1, 0.15, 0.2, 0.25, 0.3, and 0.4 g with 25 mL of 150 ppm Pb(II) solutions were used to study the effect of adsorbent weight on the adsorption capacity. For the influence of initial metal ion concentration, 0.1 g of the GO/PVF was used with 25 mL of Pb(II) solutions of different concentrations (25–300 ppm). In all experiments, the mixtures were shacked at 200 rpm for 1 h at room temperature (RT). The effect of contact time was performed by using 0.4 g of the foam with 100 mL of 200 ppm solution of Pb(II) and shacked at RT and 200 rpm. At the predetermined time, a sample of 1 mL was taken for analysis.

The adsorption capacity Q_t was estimated as follows:

$$Q_t = \frac{(C_o - C_e) \times V}{W} \quad (1)$$

where C_o (mg/L) and C_e (mg/L) are the initial and final solution concentration, respectively. V (L) is the volume of Pb(II) solution, and W (g) is the adsorbent weight. The weight of the GO inside the GO/PVF foam was used as the active weight of adsorbent. The pure PVF did not show any adsorption behavior for the Pb(II) from the aqueous solutions. The weight of the dried GO/PVF was ≈8 g. This weight contains only 0.2 g GO, accordingly, GO represents only 2.5% from the total weight of the adsorbent. Therefore, all the adsorbents weights were reduced to 2.5% from the total weight. The percentage of removal was calculated according to Eq. (2):

$$\%\ of\ \ Removal = \frac{(C_o - C_e)}{C_o} \times 100 \quad (2)$$

Fast sequential double beam atomic absorption spectrometric system (240 FS–Agilent) was used to measure Pb(II) concentration.

3. Results and discussion

3.1. Surface and structural characterization of GO and GO/PVA foams

Fig. 2(a) depicts the HRTEM image for as-prepared highly oxidized GO sheets. One can clearly observe that GO sheets have a smooth carpet-like structure. The presence of relatively large number of oxygenated functional groups on edges and surface of GO sheets facilitates the exfoliation of bulk graphite oxide to mono- or bi-layers GO [48,49]. The UV–vis spectroscopy was used to characterize the quality of oxidization and exfoliation. Fig. 2(b) shows the UV–vis spectrum of GO aqueous solution. Two characteristic peaks are shown in the spectrum. The shoulder at ≈320 nm is due to the n–π^* plasmon peak while the pronounced peak at ≈225 nm could be assigned to

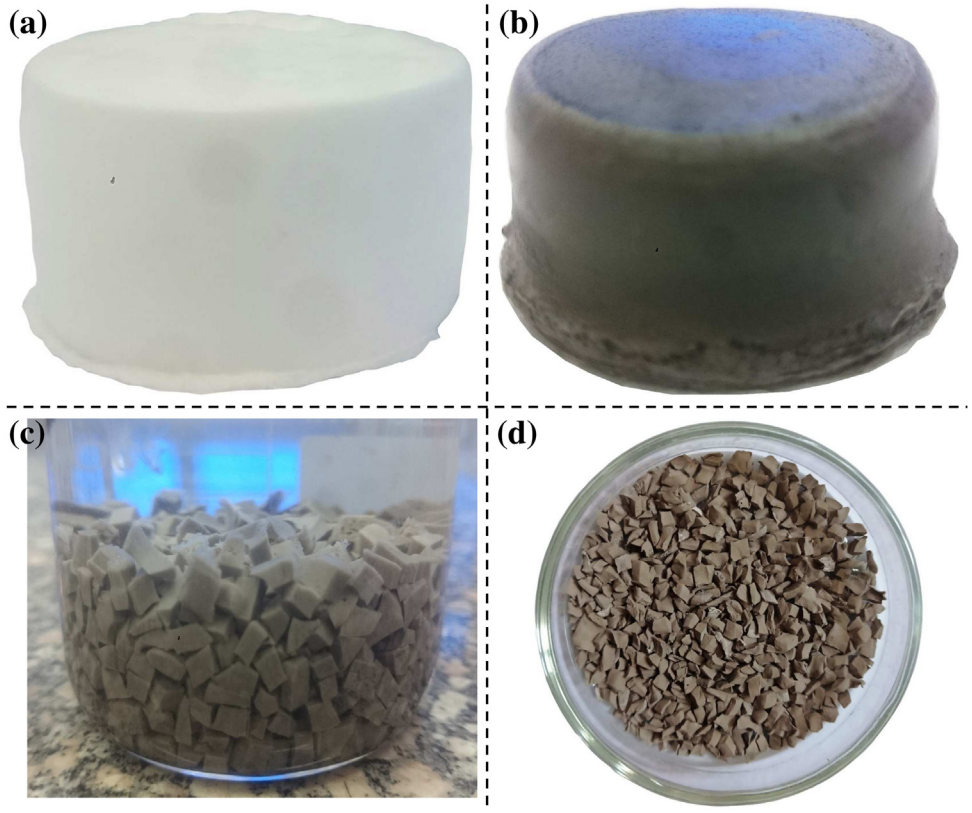

Fig. 1 – Optical images (a) as prepared pure PVF foams and (b) GO/PVF foam. The color of the GO/PVF foam changed from white to homogenous brown, indicating the homogenous distribution of the GO inside the PVF matrix after the foaming process. (c) Washing of the small pieces of GO/PVF to remove any residuals of Triton X-100 and formaldehyde. (d) Dried GO/PVF foam pieces before being used in adsorption experiments.

the π–π^* plasmon [44]. The intensity of the π–π^* plasmon peak depends on the presence of chromophore units such as C═C, C═O and C-O [50]. Here, the appearance of pronounced π–π^* plasmon peak indicates that the GO sample is highly oxidized and contains mainly mono- or bi-layers GO [44].

Raman spectra of GO, PVF, and GO/PVF are shown in Fig. 2(c) and (d), respectively. The Raman spectrum of GO sheets in Fig. 2(c), depicts the three characteristic peaks of graphite materials, namely, D-, G-, and 2D-mode at ≈1345, ≈1570, and ≈2655 cm^{-1}, respectively. The appearance of the first order G-mode is due to stretching vibration of sp^2 carbon-carbon bonds in graphitic hexagonal rings [51]. The relatively intense D-mode reflects the presence of carbon sp^3 centers due to the oxidization. The second-order 2D-mode appeared at lower frequency compared to parent bulk graphite (≈2730 cm^{-1}) indicating the presence of a few layered graphene [48,52]. The Raman spectrum of pure PVF is shown in Fig. 2(d), the peak centered at ≈2925 cm^{-1} is due to the stretching vibrations of $-CH_2$, while the peak at ≈1413 cm^{-1} could be due to the stretching vibration of -CH in the PVF chains [53]. In the case of GO/PVF, the three main characteristics peaks of GO: D-mode ≈ 1350 cm^{-1}, G-mode ≈ 1570 cm^{-1}, and 2D-mode ≈ 2660 cm^{-1} were shown. The characteristics peaks of the PVF did not appear in the GO/PVF due to the overlapping between the strong peaks of GO and PVF foam. Furthermore, as evident from Fig. 2(d), the intensity of I_D/I_G was slightly enhanced from 0.75 to 0.9 after foaming of PVF with GO sheets. Accordingly, the defects level on the GO sheet's surface increased after foaming process of PVA foam.

The FTIR spectra of GO powder, PVF, and GO/PVF are shown in Fig. 3(a),(c), and (d) respectively. In the case of GO powder, Fig. 3(a), the bands centered at ≈3445 and ≈1755 cm^{-1} could be ascribed to the O—H stretching vibration and the C═O stretching modes, respectively. The sharp band centered at ≈1635 cm^{-1} is assigned to the C═C aromatic bond. The O—H deformation and the C—O—C modes can be identified at ≈1383 cm^{-1} and ≈1078 cm^{-1}, respectively [44,54]. Fig. 3(c) shows the FTIR spectrum of the pure PVF foam. The broad absorption band in the frequency range 3250–3650 cm^{-1} is assigned to the O—H stretching mode. The symmetric stretching vibrations of the alkyl CH_2 absorption band appeared at 2925, 2851, 2772, and 2675 cm^{-1}. The O—H bending vibration appeared at 1643 cm^{-1}. The C—H bending modes can be clearly observed in the frequency range ≈1469–1353 cm^{-1}. The C—O—C—O—C stretching vibrations modes are appeared in the frequency range ≈1160–1060 cm^{-1} while the C—O—C stretching mode was detected at 1009 cm^{-1} [55,56]. After the addition of GO to PVF foam, there is no major changes in the FTIR spectrum of the GO/PVF foam (Fig. 3(d)). One can observe a broad absorption band in the frequency range 1750–1630 cm^{-1}.

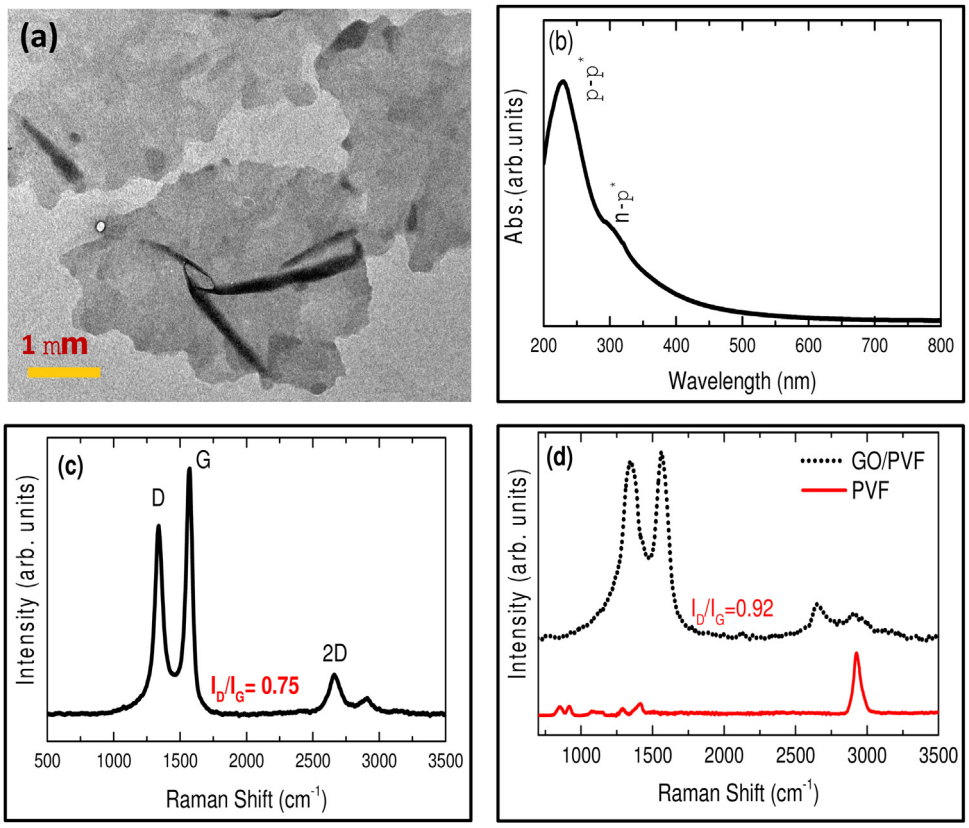

Fig. 2 – (a) HRTEM image of as prepared GO sheets. (b) UV–vis spectrum of aqueous dispersion of GO. (c) and (d) Raman spectra of GO sheets and PVF and GO/PVF foam, respectively.

This broad band consists of two distinguish bands; the band at 1750 cm^{-1} is due to C=O stretching vibration from the GO, whereas the band centered at 1640 cm^{-1} corresponding to the overlapping of the O–H bending band at 1643 cm^{-1} from the PVF and the aromatic C=C band at 1635 cm^{-1} from the GO. Also, the relative intensity of absorption bands at 1300–1475 cm^{-1} changed due to overlapping of GO absorption features with that of PVF. Accordingly, GO sheets could be attached to PVF matrix through the weak van der Waals forces [56].

The SEM image of PVF foam is shown in Fig. 4(a). The PVF foam exhibited spongy structure with open-cell interconnecting porous network. Highly irregular and deformed macroporous structure with ≈3–25 μm pore diameter with an average diameter of ≈10.8 μm (Fig. 4(c)). The formation of irregular and deformed pores could occur during drying process of the foam [57,58]. With the addition of GO into the polymeric matrix, the surface roughness and porosity significantly changed as shown in Fig. 4(b). The super-hydrophilic nature of GO sheets in aqueous solution allows them to be homogenously mixed with the PVA chains. Accordingly, during the foaming process the negatively charged layer around the GO sheets cause them to orient themselves around the foams' pores leading to a decrease in the cell-to-cell distance [59,60]. The inset of Fig. 4(b) shows that the pore diameter of the foam decreased from ≈3–25 μm to ≈6–8 μm with an average pore diameter of ≈7 μm as shown in Fig. 4(d).

3.2. *Adsorption capacity (Qt) of GO powder*

It is well known that oxygenous groups on the surface of GO sheets react with heavy metal ions via strong surface complexation [61,21], which makes GO as ideal and superior sorbent for several heavy metal ions. In general, the behavior of GO colloids is strongly affected by several parameters such as pH, particle size, and zeta potential [62,63]. Accordingly, the efficiency of heavy metals removal will also depend on the stability of GO colloids.

Fig. 5(a) shows the DLS results for GO at different pH values ranging from 3 to 12. It is well known that, DLS results give the average particle size of GO, which is less than the lateral dimensions of the 2D GO sheets [64]. One can observe from Fig. 5(a) that the GO solution is stable in the pH range from 3-7 with small increase in the average particle size as shown in the inset of Fig. 5(a). As the pH increases beyond 7, from 8 to 12, the average particle size increases with the appearance of a tails towards higher size. The stability of the GO colloidal dispersion has been also confirmed by measuring the zeta potential (ζ) for the solution at different pH values as shown in Fig. 5(b). It can be observed that the ζ increases from −27 to −60 with increasing pH values from 3 to 8. Above pH 8, the negative value of ζ decreases up to pH 12, meaning that the highest stability is obtained at pH 8, although the GO is highly stable in the pH range from 6 to 8. The photographs shown in Fig. 5(c) confirmed such reasoning. One can clearly observe that GO solutions are stable without any noticeable aggregates

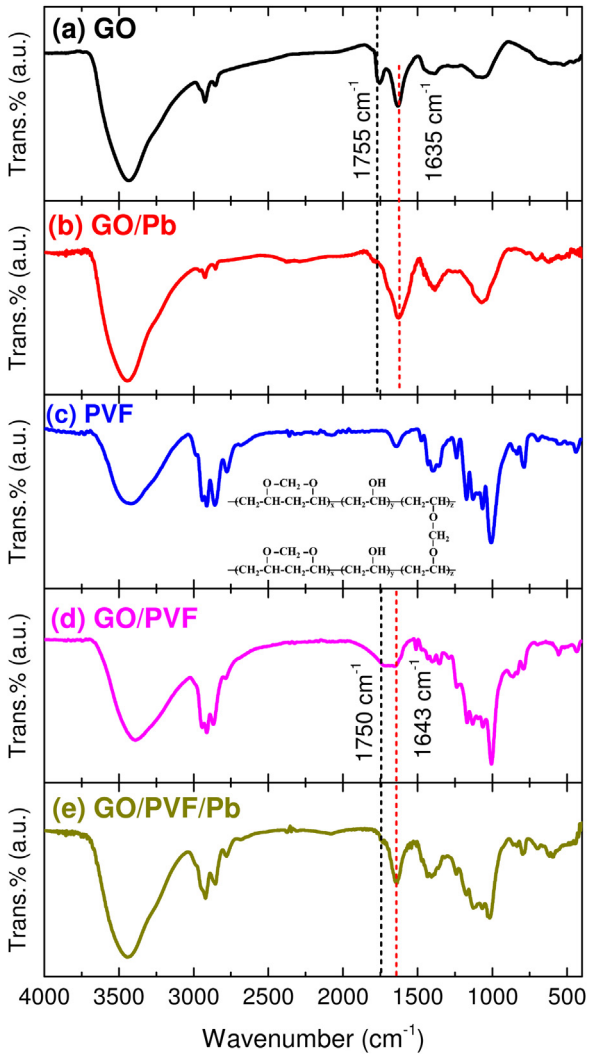

Fig. 3 – FT-IR spectra of (a) GO powder, (b) GO loaded with Pb(II) (GO/Pb), (c) PVF foam, (d) GO/PVF foam, and (e) GO/PVF loaded with Pb(II) (GO/PVF/Pb) in the range between 4000 and 400 cm^{-1}. The vertical dashed lines identify the peak positions of the C=O, and C=C bonds.

for pH values up to 7 where in the pH range 8–12 GO sheets form visible aggregates. It is well known that addition of NaOH has the ability to clean the oxidation debris present on the surface of GO sheets [65]. The removal of these debris from the GO surface reduce the oxygen functionalities from GO surface forming graphene-like sheets with less oxygen content compared with the untreated GO. These graphene-like sheets stabilizes themselves in solutions by reducing their effective size. In the pH range from 8 to 12, the relatively large particle distribution can be attributed to salting out effect of the NaOH additives [63].

The adsorption of Pb(II) on GO powder was investigated at different pH values. Here, 2.5 mL of GO solution of 1 mg/mL concentration was added to 25 mL of 150 ppm Pb(II) solution. The weight of 2.5 mg of GO is the weight present in 0.1 g of GO/PVF foam. This weight of GO/PVF foam was the optimum weight giving maximum adsorption capacity of Pb(II). Please, see Section 3.3 for more details.

As shown in Fig. 5(d), as the pH value increases from 2 to 6, the adsorption of Pb(II) increased and then decreased again at pH > 6. In general, the adsorption of Pb(II) on the surface of GO was ascribed to ion exchange of Pb(II) with H^+ [21]. It is well known that, the Pb(II) are present in solutions in the form of Pb(II), $Pb(OH)^+$, $Pb(OH)_2^0$, $Pb(OH)_3^-$ species at different pH values [66]. The predominated species of Pb(II) at lower pH values are Pb(II) and $Pb(OH)^+$, these species replace the H^+ from oxygenated functional groups on the surface of GO sheets. Accordingly, at the low pH values, the H^+ ions compete with Pb(II) and $Pb(OH)^+$ to occupy the negative active sites available on the adsorbent leading to a decrease of the Q_t value. By increasing pH value, the concentration of H^+ will decrease and the tendency of Pb(II) to occupy active sites will increase leading to an increase of Q_t of GO. On the other hand, by raising the pH value over the optimum point, pH 6, the predominant metal ions are $Pb(OH)_3^-$. These negatively charged ions cannot be adsorbed on the negatively charged surface of

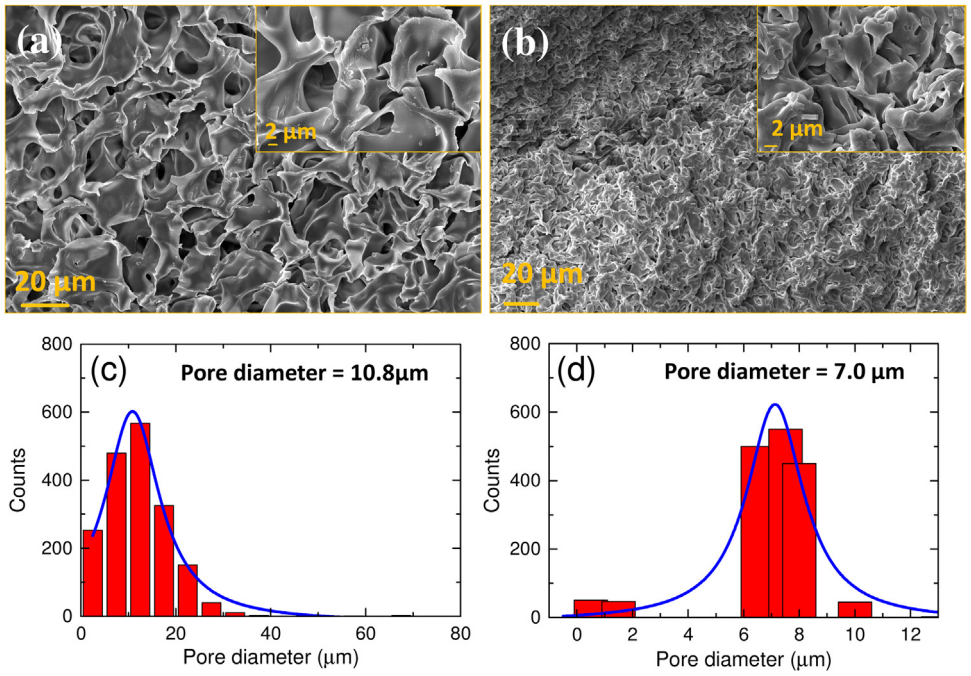

Fig. 4 – HRSEM images of (a) as prepared pure PVF foam and (b) GO/PVF foam. (c) and (d) histograms of the average pore diameter for PVF and GO/PVF foams, respectively.

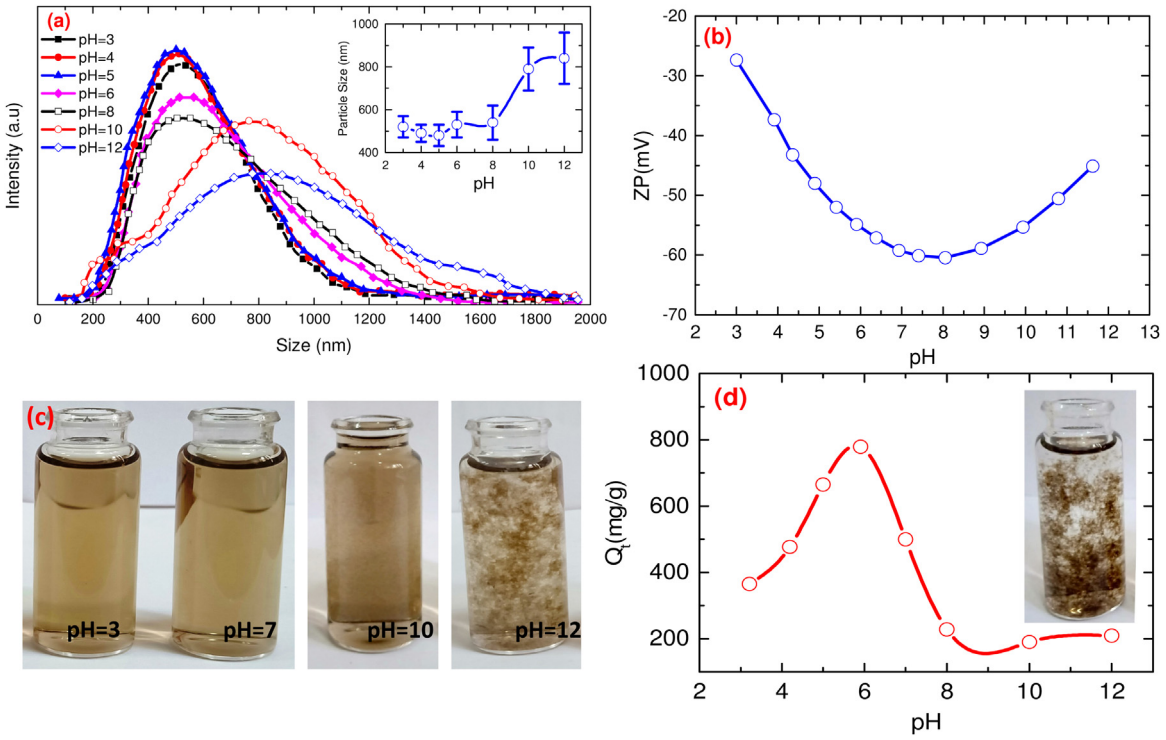

Fig. 5 – (a) Particle size distribution and (b) Zeta potential of GO colloid at different pH. Inset of (a): the average particle size at different pH. (c) Photographs showing the stability of GO colloid at different pH. (d) Adsorption capacity (Q_t) of GO toward Pb(II) using 2.5 mg in 25 mL of 150 ppm Pb(II). Inset: Photograph for the Pb(II) solution after 10 min from the addition of GO.

GO sheets. Therefore, at pH value more than 6, the Q_t of GO will be decreased [21,67].

From Fig. 5(d), one can observe that Q_t of Pb(II) on GO was ≈800 mg g^{-1} at pH 6. According to previously published results [14,21,22], GO showed several adsorption capacities values for Pb(II) based on functionalization level and type. In comparison to previously published results on the Q_t of Pb(II) on GO sheets, our sample efficiency is very close to that of the highest three currently published data: 842 mg g^{-1} [21], 931 mg g^{-1} [14], and 1119 mg g^{-1} [22]. The variations in the adsorption capacities could be attributed to the degree of functionalization of GO. The presence of plenty of reactive functional groups on GO surface enhances its adsorption capacity.

It is well known that GO form a very stable suspension in water for long time. The long term stability of GO sheets in water could be ascribed to the electrostatic repulsions between negatively charged oxygenated groups. However, the stable dispersibility of GO changes remarkably with the addition of metal ions to GO solutions where GO tends to form agglomerates. The negatively charged functional groups on GO surface create metal-GO complex with Pb ions causing agglomeration of GO sheets [22]. As the interaction between the Pb ions and GO starts, the density of GO sheets was increased and the precipitation was observed. This is shown in the inset of Fig. 5(d), after the addition of GO to the Pb(II) solution, the GO sheets formed agglomerates after few minutes (≈10 min).

Fig. 3(b) shows the FTIR spectrum of GO loaded with Pb(II) (GO/Pb). After the adsorption of Pb(II) on GO, there is no significant changes in the FTIR spectrum of the GO/Pb were observed, expect the disappearance of the C=O mode which appeared at 1755 cm^{-1} in the case of GO powder (Fig. 3(a)). This could be due to the formation of metal-GO complex as bond generated between Pb(II) and oxygenated groups on the GO sheets [22].

Accordingly, due to the agglomerate of GO sheets the effective surface area and the efficiency of heavy metals removal reduced. If the GO sheets remain stable without any agglomeration during the interaction between heavy metal ions and GO sheets, the adsorption capacity is expected to grow up to higher values. To test this idea, GO sheets were incorporated into PVF matrix for immobilization and avoiding their agglomeration during the interaction with Pb(II).

3.3. *Adsorption capacity (Qt) of GO/PVF foam*

Fig. 6(a) show the SEM image of GO/PVF loaded with Pb crystals. After the adsorption experiment, one can observe aggregations of lead crystals on the surface of GO/PVF foam. These crystals were confirmed by EDX analysis (Fig. 6(c)). The distribution of Pb(II) on the surface of GO/PVF foam was investigated by the elemental mapping of the foam's surface after adsorption of Pb(II) (Fig. 6(b)). The mapping image shows that Pb crystals are homogenously distributed on the surface of GO/PVA foam. This could be attributed to homogenous distribution of the GO sheets inside the PVF matrix. Moreover, the Pb percentage was calculated from EDX results which equal to 6.36% as shown Fig. 6(d).

The FTIR spectrum of PVF loaded with Pb crystals (PVF/GO/Pb) is shown in Fig. 3(e). As in the case of GO/Pb, no major changes in the FTIR spectrum of the foam was observed except the band at 1750 cm^{-1} which was assigned to the C=O stretching vibration disappeared. In addition, the intensity of the C—O—C at 1009 cm^{-1} decreased. This could be attributed to the complexation reaction between lead ions to oxygenated functional groups present on GO sheets.

To examine the absorption capacity of the prepared foams, several factors have been tested such as pH, initial adsorbent dosage, initial concentration of the Pb(II), and contact time. The pure PVF foam did not show any adsorption affinity for the Pb(II) under any applied conditions, accordingly, the adsorption of Pb (II) are due to the introduction of GO into the PVF polymeric matrix.

3.3.1. *Effect of pH*

It is well known that the pH value has a great effect on the Q_t of metal ions in solutions. The relation between Q_t (mg g^{-1}) and pH value of the solution is shown in Fig. 7(a). As the pH increases, the adsorption of Pb(II) is grown until reaching a maximum value of 600 mg g^{-1} at pH 5 and then the Pb(II) removal capacity was reduced at pH higher than 6. The effect of pH value on the Q_t of Pb(II) on GO sheets was explained in details in Section 3.2. The same explanation holds here since the main active sites available for adsorption is the oxygenated functional groups on the surface of GO sheets.

3.3.2. *Effect of initial adsorbent dosage*

Fig. 7(b) shows the Q_t as a function of initial adsorbent weight at optimum pH value, i.e., pH 5. One can clearly observe that as the initial dosage of the adsorbent increases the Q_t values are increased until it reaches a maximum value of 1300 mg g^{-1} at adsorbent dose of 0.1 g. Then the Q_t abruptly declines with further increase of adsorbent dose higher than 0.1 g. This can be explained as follows: (i) by increasing the adsorbent dose, the number of available adsorbing sites is increased but with constant amount of Pb(II) the adsorbed ions per unit mass decreases and hence the total Q_t decreases [68]. (ii) The adsorbed ions on the foam surface may block other ions from reaching the internal pores of adsorbent leading to a decrease of the number of available active sites for further adsorption, i.e., adsorption sites remaining unsaturated during the adsorption reaction [69].

3.3.3. *Effect of initial metal ion concentration*

Fig. 7(c) depicts the relation between the initial Pb(II) concentration and the adsorption capacity Q_t at optimum conditions of pH 5 and adsorbent weight of 0.1 g. It was found that, by increasing Pb(II) concentration, the adsorption capacity is increased until it reached a maximum value of 1666 mg g^{-1} at 200 ppm, after that the value is decreased with the amount of Pb(II) higher than 200 ppm. At low Pb(II) concentrations all the existing ions can be adsorbed on the available active sites on GO sheets. By raising the ions concentration in the solution, most of the free active sites on the adsorbent surface may be occupied with Pb(II) leading to a decrease of the adsorption capacity [70]. The corresponding removal efficiency is shown in Fig. 7(d).

3.3.4. *Study of the contact time*

For studying the effect of contact time on the Q_t, all optimum parameters were set, i.e., pH 5, adsorbent weight 0.1 g, and

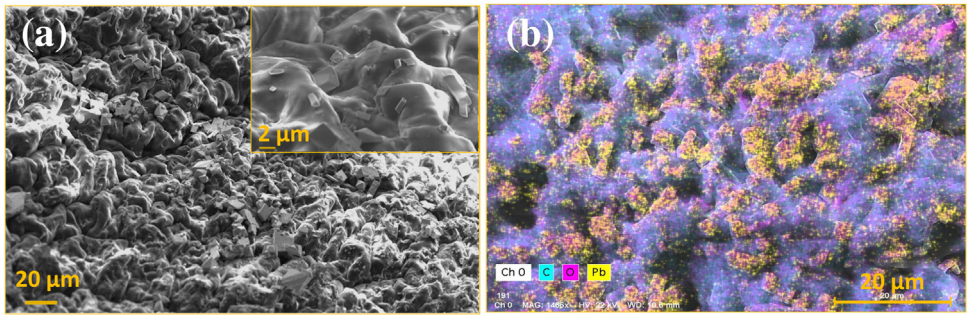

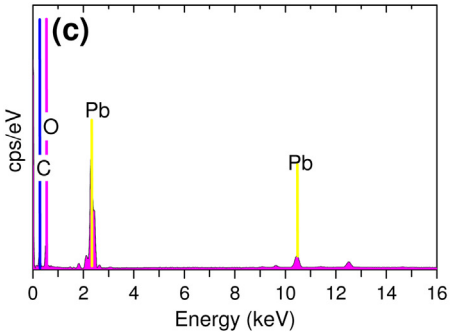

(d)

Element	Atom	abs. error%	Rel. error %
Carbon	55.92	2.29	13.1
Oxygen	37.72	2.06	12.98
lead	6.36	0.89	2.73
sum	100		

Fig. 6 – HRSEM images of (a) GO/PVF foam loaded with Lead crystals and (b) elemental mapping of the GO/PVF foam loaded with Lead crystals. (c) The energy dispersive X-ray (EDX) elemental analysis of GO/PVF foam loaded with Lead crystals. (d) Percentage of elements present in the GO/PVF foam calculated from the EDX analysis.

Table 1 – Comparison between the maximum Q_t values of Pb(II) ions on different sorbents.

Sorbents	Q_t(max) (mg g^{-1})	pH, temp. (K)	No. of cycles	Ref. no.
Activated carbon	25.5	6.0, 303	N/A	[71]
MWCNTs	97	5.0, 303	N/A	[81]
2- or 3-layered graphene	400	6.0, 298	N/A	[21]
Highly oxidized GO	932–1119	5, 298	N/A	[14,22]
GNS^{PF6}	400	5.0, 303	5 cycles	[18]
EDTA-GO	479	6.8, 303	10 cycles	[19]
GO-$MnFe_2O_4$	673	6.0, 303	More than 5 cycles	[20]
Conjugated adsorbents	175–204	5.5, 303	7–8 cycles	[82–84]
polysiloxane/GO sponge	256.41	5, 313	5 cycles	[36]
GO/melamine sponge	349.7	6, 303	5 cycles	[40]
GO	800	6.0, 298	N/A	This work
GO/PVF foam	1730	5.0, 298	10 cycles	This work

initial ion concentration of 200 ppm. The contact time experiment was performed in time range from 10 to 180 min. Fig. 7(e) shows the relation between the Q_t and the contact time t (min). It is clear that the Q_t is dramatically increased by increasing the contact time till it reaches a maximum value of 1730 mg g^{-1} at 90 min at which the equilibrium between metal ions and active sites is achieved. After the equilibrium point the Q_t is slightly increased followed by a plateau above 90 min. From the optimized conditions, it can be concluded that the immobilization of GO sheets inside PVF polymeric matrix enhanced the Q_t to reach 1730 mg g^{-1} at pH 5 after 90 min. As it was explained in Section 3.2, the PVF matrix acts as stabilizer for the GO sheets and prevents their agglomeration during the interaction between Pb(II) and the oxygenated functional groups leading to the increase of the Q_t values from 800 to 1730 mg g^{-1}. Here, the adsorption capacity of GO is close to the previously published data. Surprisingly, the Q_t value in case of GO inside PVF matrix is the highest of today's adsorbents materials, as listed in Table 1.

3.4. *Adsorption kinetics*

For kinetic and isotherm studies, solutions of metal ion of 100, 200, 300, and 400 ppm concentrations were prepared and tested at time ranged from 10 to 180 min while all optimum conditions were set constant. The adsorption process mechanism of heavy metal ions on sorbent active sites is governed by many factors such as, applied conditions, adsorbents physical form, and metal ion properties. To determine the maximum adsorption capacity the obtained adsorption data is formulated in a certain kinetic models. The most common models used are (1) pseudo-first-order, (2) pseudo-second-order, and (3) intraparticle diffusion model [71].

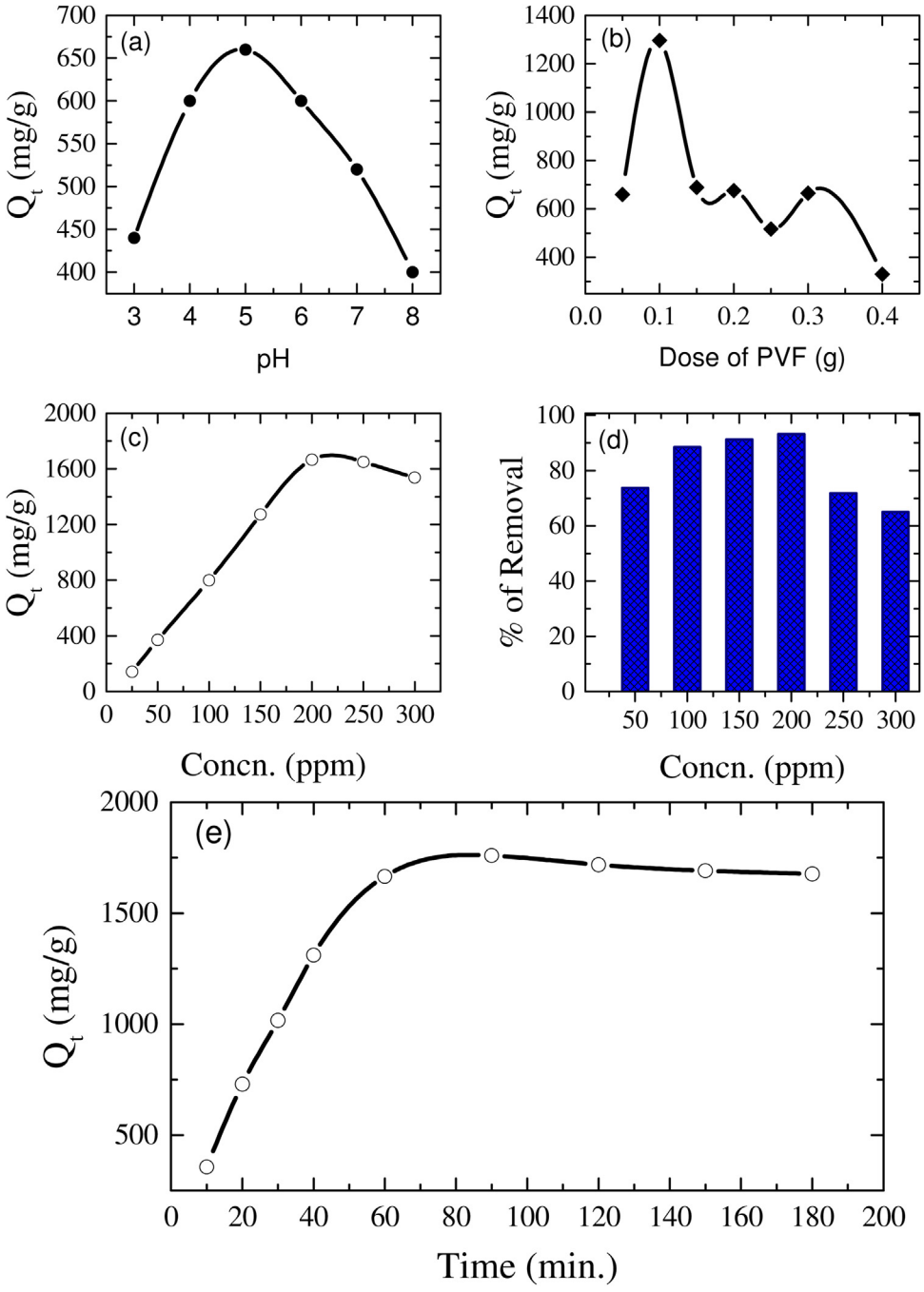

Fig. 7 – Factors affecting the adsorption capacity (Q_t) of GO/PVF foam (a) the effect of pH value using 0.05 g of GO/PVF. (b) Initial adsorbent dosage effect at optimum pH value, i.e., pH 5. (c) Initial metal ion concentration effect and (d) percentage of removal at optimum conditions of pH 5, 0.1 g of PVF, and 25 mL Pb(II). (e) The effect of contact time on the adsorption capacity of the GO/PVF foam.

The pseudo-first-order and second-order kinetic models can be described by the following equations:

$$\log[q_e - q_t] = \log[q_e] - \left[\frac{K_1}{2.303}\right] t \quad (3)$$

$$\frac{t}{q_t} = \frac{1}{K_2 \times q_e^2} + \frac{t}{q_e} \quad (4)$$

where q_e (mg g^{-1}) and q_t (mg g^{-1}) are the adsorption values at equilibrium and pre-determined time t, respectively. K_1 (min^{-1}) and K_1 (min^{-2}) are the pseudo-first- and pseudo-second-order kinetic model rate constant, respectively. The linear plots representing both models are shown in Fig. 8(a) and (b). The calculated values of the pseudo-first-order model parameters are as follows: $q_e = 3020$ mg g^{-1}, $K_1 = 0.0445$ min^{-1}, and $R^2 \approx 0.961$ and the values for the case of

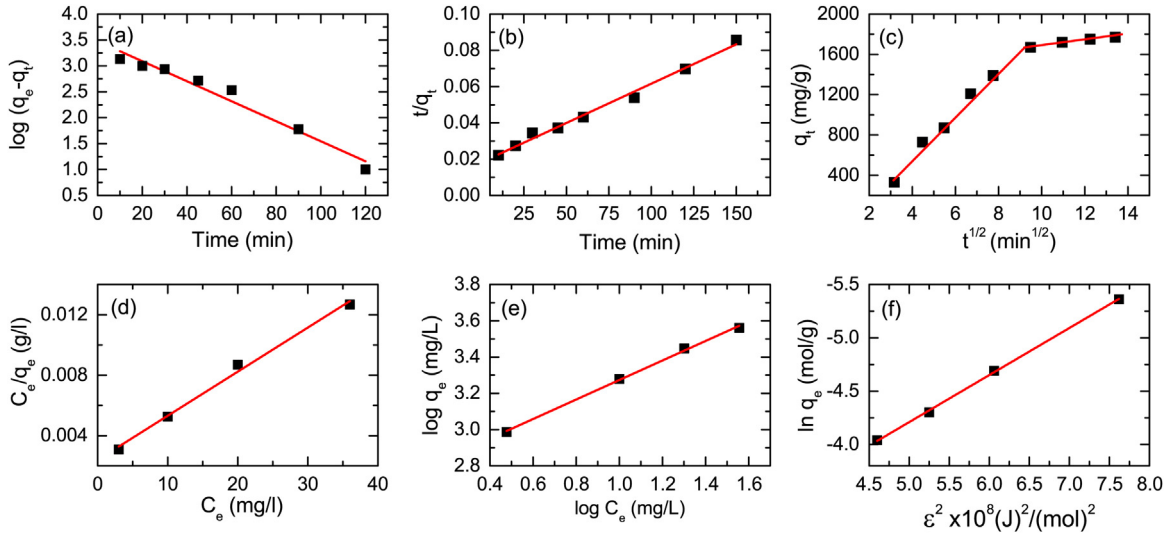

Fig. 8 – (a) Pseudo first-order, (b) pseudo second-order, (c) intraparticle diffusion, (d) Langmuir isotherm, (e) Freundlich model, and (f) Dubinin–Kaganer–Radushkevich (DKR) models for the adsorption of Pb(II) on the PVF/GO foam.

pseudo-second-order model parameters are: $q_e = 1900\,mg\,g^{-1}$, $K_2 = 1.38 \times 10^{-5}\,min^{-1}$, and $R^2 \approx 0.989$.

From the calculated values, it can be concluded that the adsorption of Pb(II) on PVF/GO foam is mostly fitted with the pseudo-second order model as the R^2 value is ≈0.989 and the theoretical value of q_e is in a good agreement with the calculated one. Accordingly, the adsorption of Pb(II) on the surface of PVF/GO foam could be occurred through chemical adsorption [72,73].

For the case of intraparticle diffusion model, the adsorption of Pb(II) on a surface of porous sorbent can be occurred through many steps such as exterior, interior pore, and surface diffusion. The diffusion mechanisms of the overall process can be occurred by one or more of these steps. The intraparticle diffusion model can be described by the following equation:

$$q_t = K_{int} \times t^{1/2} \tag{5}$$

Fig. 8(c) shows the relation between q_t and $t^{1/2}$. The adsorption process is one rate-limiting step when the relation between q_t and $t^{1/2}$ is a straight line passes through the origin [74]. If the graph is divided into more than one linear sections then there are more than one step occurred [75]. From Fig. 8(c), It is clear that the intraparticle diffusion model graph exhibits a linear plot with two separate well defined linear sections indicating that the diffusion of metal ions into the porous material occurs in two stages. In the first stage, the adsorption process increased gradually controlled by the intraparticle diffusion until equilibrium; second stage, at which the concentration of metal ions in the solution is decreased leading to slowing down the metal diffusion through the pours of the foam [75].

3.5. *Isotherm*

During heavy metal ion adsorption process by using solid sorbent, isotherm models must be applied to investigate the uptake behavior of Pb(II) from the solution medium on the surface of GO/PVF foam. The well-known isotherm models used to describe the possible sorption processes are Langmuir, Freundlich, and Dubinin–Kaganer–Radushkevich (DKR) sorption isotherms. The Pb(II) uptake was studied as a function of initial concentrations in the solution from 100 to 400 ppm while all other optimum parameters were kept constant.

Langmuir isotherm model suggested that the adsorption of heavy metal ions on sorbent surface is a monolayer sorption process with limited number of homogenous sites [76]. The model can be represented as follows:

$$\frac{C_e}{q_e} = \frac{1}{Kq_{max}} + \frac{C_e}{q_{max}} \tag{6}$$

where C_e (mg/L) represents the equilibrium concentration of the Pb(II) in solution, q_e ($mg\,g^{-1}$) is the amount of adsorbed ions at equilibrium, q_{max} ($mg\,g^{-1}$) and K are the maximum sorption capacity and affinity of adsorption, respectively. The calculated values of the Langmuir parameters are $q_{max} = 3428\,mg\,g^{-1}$, $K = 0.121$ L/mg, and $R^2 = 0.9971$.

Freundlich model is used to describe the characteristics of the sorption process for a heterogenous surface [77]. Eq. (7) represents the simplified form of Freundlich model:

$$\log q_e = \log K_f + \frac{1}{n} \log C_e \tag{7}$$

where n and K_f are adsorption intensity and capacity, respectively. Fig. 8(d) and (e) show the liner plots representing both Langmuir and Freundlich models, respectively. The calculated Freundlich model parameters are $K_f = 543$, $1/n = 0.538$, and $R^2 = 0.9973$.

To study the sorption mechanism of the process, DKR isotherm model is used predominantly over Langmuir and Freundlich isotherms models. DKR can be considered as an analogue form of Langmuir model but it does not suggest a

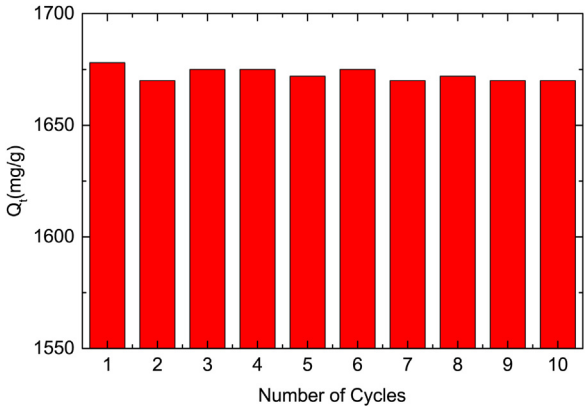

Fig. 9 – The relation between the number of cycles and the maximum adsorption capacity of the GO/PVF foam using 0.1 mg GO/PVF foam, pH 5, and 90 min contact time.

homogenous surface [78,79]. Eq. (8) shows the linearized form of the DKR isotherm model:

$$\ln q_e = \ln X_m - \beta\varepsilon^2 \tag{8}$$

where q_e (mol/g) is the number of adsorbed ions per unit adsorbent weight, X_m (mol/g) is the maximum sorption capacity, β (mol^2/J^2) is the activity coefficient, and ε is the Polanyi potential (J/mol). Fig. 8(f) shows the plot of $\ln q_e$ versus ε^2. The slope of the line gives the value of β (4.41×10^{-9} mol^2/J^2) and the intercept gives the sorption capacity X_m (13.5×10^{-2} mol/g).

According to Eq. (9), the value of the sorption energy is 10.65 kJ/mole. The positive value of E indicates that the process is endothermic and the mechanism of reaction is an ion-exchange [67]:

$$E = \frac{1}{\sqrt{-2\beta}} \tag{9}$$

The results reveal that the uptake process is best described by the Freundlich model, as $1/n$ value is 0.538, and R^2 is 0.9992. These results predict that the adsorption process of Pb(II) on GO/PVF was done on a heterogenous surface. Moreover, for DKR model the results show that the values of E was 10.65 kJ/mol ($8 < E < 16$ kJ/mol), indicating that the mechanism is ion exchange reaction [79,80].

3.6. *Desorption and regeneration*

To study the reusability of the prepared material GO/PVF foam, the loaded composite were soaked in 10% H_2SO_4 solution for 60 min, then the foam washed several time with water till the pH reached ≈7. Another adsorption experiment was performed using 0.1 mg GO/PVF foam and all the optimum conditions were kept constant. As shown in Fig. 9, the PVF/GO foam has an excellent adsorption capacity of ≈1730 mg g^{-1} up to 10 cycles. The physical and mechanical properties of such foam did not change significantly after the end of the reusability test indicating the high economic value of the GO/PVF foam in addition to superior and eco-friendly properties of the foam.

4. Conclusions

In this study, GO/PVF foam with excellent mechanical and chemical stability was successfully prepared via traditional PVA acetylation reaction. The developed foam proved to be a promising adsorbent material for Pb(II) removal. The Q_t of GO is increased from 800 to 1730 mg g^{-1} when immobilized inside PVF foam matrix. The PVF matrix prevented the agglomeration of GO sheets during the adsorption of Pb(II). The excellent dispersibility of GO sheets inside the PVF matrix facilities the formation of GO metal bonds. The Q_t of immobilized GO sheets inside PVF matrix is the highest of today's adsorbents materials. The extensive study of kinetic models reveals that the adsorption mechanism of the prepared GO/PVF foam is fitted with the pseudo-second-order model and the process was occurred as ion exchange reaction. Furthermore, the Freundlich model is the best describing adsorption isotherm process, which proved that the adsorption process was done on the heterogenous surface. Moreover, the prepared foam can be re-used up to 10 times, with almost the same removal efficiency without any significant changes in its physical feathers. Here, the fascinating adsorptive properties of the GO/PVF foam could increase this sorbent in the field of water treatment, preconcentration, and separation of trace-metal ions.

Conflicts of interest

The authors declare no conflicts of interest.

Acknowledgements

We acknowledge financial support by the Science and Technology Development Fund (STDF), Egypt, project ID 25610. Ahmed S.G. Khalil acknowledges the financial support from the Arab-German Young Academy of Sciences and Humanities (AGYA).

REFERENCES

[1] Ghorbani M, Seyedin O, Aghamohammadhassan M. Adsorptive removal of lead (II) ion from water and wastewater media using carbon-based nanomaterials as unique sorbents: a review. J Environ Manag 2020;254:109814, http://dx.doi.org/10.1016/j.jenvman.2019.109814.

[2] Jawed A, Saxena V, Pandey LM. Engineered nanomaterials and their surface functionalization for the removal of heavy metals: a review. J Water Process Eng 2020;33:101009, http://dx.doi.org/10.1016/j.jwpe.2019.101009.

[3] Yousefi N, Lu X, Elimelech M, Tufenkji N. Environmental performance of graphene-based 3D macrostructures. Nat Nanotechnol 2019;14(2):107–19, http://dx.doi.org/10.1038/s41565-018-0325-6.

[4] Fu F, Wang Q. Removal of heavy metal ions from wastewaters: a review. J Environ Manag 2011;92(3):407–18, http://dx.doi.org/10.1016/j.jenvman.2010.11.011.

[5] Eloussaief M, Benzina M. Efficiency of natural and acid-activated clays in the removal of Pb(II) from aqueous solutions. J Hazard Mater 2010;178(1):753–7, http://dx.doi.org/10.1016/j.jhazmat.2010.02.004.

[6] Gupta V, Saleh TA. Syntheses of carbon nanotube-metal oxides composites; adsorption and photo-degradation. In: Bianco S, editor. Carbon nanotubes – from research to applications. Intech Open; 2011. p. 295–312. ISBN 978-953-307-500-6.
[7] Bolisetty S, Peydayesh M, Mezzenga R. Sustainable technologies for water purification from heavy metals: review and analysis. Chem Soc Rev 2019;48:463–87, http://dx.doi.org/10.1039/C8CS00493E.
[8] Awual MR, Hasan MM. A ligand based innovative composite material for selective lead(II) capturing from wastewater. J Mol Liq 2019;294:111679, http://dx.doi.org/10.1016/j.molliq.2019.111679.
[9] Awual MR. Mesoporous composite material for efficient lead(II) detection and removal from aqueous media. J Environ Chem Eng 2019;7(3):103124, http://dx.doi.org/10.1016/j.jece.2019.103124.
[10] Awual MR. Efficient phosphate removal from water for controlling eutrophication using novel composite adsorbent. J Clean Prod 2019;228:1311–9, http://dx.doi.org/10.1016/j.jclepro.2019.04.325.
[11] Awual MR, Rahman IM, Yaita T, Khaleque MA, Ferdows M. pH dependent Cu(II) and Pd(II) ions detection and removal from aqueous media by an efficient mesoporous adsorbent. Chem Eng J 2014;236:100–9, http://dx.doi.org/10.1016/j.cej.2013.09.083.
[12] Bassyouni M, Mansi AE, Elgabry A, Ibrahim BA, Kassem OA, Alhebeshy R. Utilization of carbon nanotubes in removal of heavy metals from wastewater: a review of the CNTs' potential and current challenges. Appl Phys A 2019;126(1):38, http://dx.doi.org/10.1007/s00339-019-3211-7.
[13] Wang X, Nie S, Zhang P, Song L, Hu Y. Superhydrophobic and superoleophilic graphene aerogel for ultrafast removal of hazardous organics from water. J Mater Res Technol 2020;9(1):667–74, http://dx.doi.org/10.1016/j.jmrt.2019.11.008.
[14] Zhang J, Li Y, Xie X, Zhu W, Meng X. Fate of adsorbed Pb(II) on graphene oxide under variable redox potential controlled by electrochemical method. J Hazard Mater 2019;367:152–9, http://dx.doi.org/10.1016/j.jhazmat.2018.12.073.
[15] Jia J, Huang G, Deng J, Pan K. Skin-inspired flexible and high-sensitivity pressure sensors based on rGO films with continuous-gradient wrinkles. Nanoscale 2019;11:4258–66, http://dx.doi.org/10.1039/C8NR08503J.
[16] Liu X, Ma R, Wang X, Ma Y, Yang Y, Zhuang L, et al. Graphene oxide-based materials for efficient removal of heavy metal ions from aqueous solution: a review. Environ Poll 2019;252:62–73, http://dx.doi.org/10.1016/j.envpol.2019.05.050.
[17] Zhang C, Luan J, Yu X, Chen W. Characterization and adsorption performance of graphene oxide – montmorillonite nanocomposite for the simultaneous removal of Pb^{2+} and p-nitrophenol. J Hazard Mater 2019;378:120739, http://dx.doi.org/10.1016/j.jhazmat.2019.06.016.
[18] Deng X, Lü L, Li H, Luo F. The adsorption properties of Pb(II) and Cd(II) on functionalized graphene prepared by electrolysis method. J Hazard Mater 2010;183(1):923–30, http://dx.doi.org/10.1016/j.jhazmat.2010.07.117.
[19] Madadrang CJ, Kim HY, Gao G, Wang N, Zhu J, Feng H, et al. Adsorption behavior of EDTA-graphene oxide for Pb (II) removal. ACS Appl Mater Interfaces 2012;4(3):1186–93, http://dx.doi.org/10.1021/am201645g.
[20] Kumar S, Nair RR, Pillai PB, Gupta SN, Iyengar MAR, Sood AK. Graphene oxide-$MnFe_2O_4$ magnetic nanohybrids for efficient removal of lead and arsenic from water. ACS Appl Mater Interfaces 2014;6(20):17426–36, http://dx.doi.org/10.1021/am504826q.
[21] Zhao G, Ren X, Gao X, Tan X, Li J, Chen C, et al. Removal of Pb(II) ions from aqueous solutions on few-layered graphene oxide nanosheets. Dalton Trans 2011;40:10945–52, http://dx.doi.org/10.1039/C1DT11005E.
[22] Sitko R, Turek E, Zawisza B, Malicka E, Talik E, Heimann J, et al. Adsorption of divalent metal ions from aqueous solutions using graphene oxide. Dalton Trans 2013;42:5682–9, http://dx.doi.org/10.1039/C3DT33097D.
[23] Akram MY, Ahmed S, Li L, Akhtar N, Ali S, Muhyodin G, et al. N-doped reduced graphene oxide decorated with Fe_3O_4 composite: stable and magnetically separable adsorbent solution for high performance phosphate removal. J Environ Chem Eng 2019;7(3):103137, http://dx.doi.org/10.1016/j.jece.2019.103137.
[24] Cheminski T, de Figueiredo Neves T, Silva PM, Guimar aes CH, Prediger P. Insertion of phenyl ethyleneglycol units on graphene oxide as stabilizers and its application for surfactant removal. J Environ Chem Eng 2019;7(2):102976, http://dx.doi.org/10.1016/j.jece.2019.102976.
[25] Prediger P, Cheminski T, de Figueiredo Neves T, Nunes WB, Sabino L, Picone CSF, et al. Graphene oxide nanomaterials for the removal of non-ionic surfactant from water. J Environ Chem Eng 2018;6(1):1536–45, http://dx.doi.org/10.1016/j.jece.2018.01.072.
[26] Othman NH, Alias NH, Shahruddin MZ, Bakar NFA, Him NRN, Lau WJ. Adsorption kinetics of methylene blue dyes onto magnetic graphene oxide. J Environ Chem Eng 2018;6(2):2803–11, http://dx.doi.org/10.1016/j.jece.2018.04.024.
[27] Saha S, Venkatesh M, Basu H, Pimple MV, Singhal RK. Recovery of gold using graphene oxide/calcium alginate hydrogel beads from a scrap solid state detector. J Environ Chem Eng 2019;7(3):103134, http://dx.doi.org/10.1016/j.jece.2019.103134.
[28] Jia PP, Sun T, Junaid M, Yang L, Ma YB, Cui ZS, et al. Nanotoxicity of different sizes of graphene (G) and graphene oxide (GO) in vitro and in vivo. Environ Pollut 2019;247:595–606, http://dx.doi.org/10.1016/j.envpol.2019.01.072.
[29] Liu H, Qiu H. Recent advances of 3D graphene-based adsorbents for sample preparation of water pollutants: a review. Chem Eng J 2020;393:124691, http://dx.doi.org/10.1016/j.cej.2020.124691.
[30] Qiu B, Xing M, Zhang J. Recent advances in three-dimensional graphene based materials for catalysis applications. Chem Soc Rev 2018;47:2165–216, http://dx.doi.org/10.1039/C7CS00904F.
[31] Teng J, Zeng X, Xu X, Yu JG. Assembly of a novel porous 3D graphene oxide-starch architecture by a facile hydrothermal method and its adsorption properties toward metal ions. Mater Lett 2018;214:31–3, http://dx.doi.org/10.1016/j.matlet.2017.11.072.
[32] Lai KC, Lee LY, Hiew BYZ, Thangalazhy-Gopakumar S, Gan S. Facile synthesis of xanthan biopolymer integrated 3D hierarchical graphene oxide/titanium dioxide composite for adsorptive lead removal in wastewater. Bioresour Technol 2020:123296, http://dx.doi.org/10.1016/j.biortech.2020.123296.
[33] Luo J, Fan C, Xiao Z, Sun T, Zhou X. Novel graphene oxide/carboxymethyl chitosan aerogels via vacuum-assisted self-assembly for heavy metal adsorption capacity. Colloids Surf A: Physicochem Eng Aspects 2019;578:123584, http://dx.doi.org/10.1016/j.colsurfa.2019.123584.
[34] Wu Z, Deng W, Zhou W, Luo J. Novel magnetic polysaccharide/graphene oxide @Fe3O4 gel beads for adsorbing heavy metal ions. Carbohydr Polymers 2019;216:119–28, http://dx.doi.org/10.1016/j.carbpol.2019.04.020.

[35] Gao H, Sun Y, Zhou J, Xu R, Duan H. Mussel-inspired synthesis of polydopamine-functionalized graphene hydrogel as reusable adsorbents for water purification. ACS Appl Mater Interfaces 2013;5(2):425–32, http://dx.doi.org/10.1021/am302500v.
[36] Zhou G, Liu C, Tang Y, Luo S, Zeng Z, Liu Y, et al. Sponge-like polysiloxane-graphene oxide gel as a highly efficient and renewable adsorbent for lead and cadmium metals removal from wastewater. Chem Eng J 2015;280:275–82, http://dx.doi.org/10.1016/j.cej.2015.06.041.
[37] Xu X, Zou J, Zhao XR, Jiang XY, Jiao FP, Yu JG, et al. Facile assembly of three-dimensional cylindrical egg white embedded graphene oxide composite with good reusability for aqueous adsorption of rare earth elements. Colloids Surf A: Physicochem Eng Aspects 2019;570:127–40, http://dx.doi.org/10.1016/j.colsurfa.2019.03.022.
[38] Xu X, Zou J, Teng J, Liu Q, Jiang XY, Jiao FP, et al. Novel high-gluten flour physically cross-linked graphene oxide composites: Hydrothermal fabrication and adsorption properties for rare earth ions. Ecotoxicol Environ Saf 2018;166:1–10, http://dx.doi.org/10.1016/j.ecoenv.2018.09.062.
[39] Xu X, Jiang XY, Jiao FP, Chen XQ, Yu JG. Tunable assembly of porous three-dimensional graphene oxide-corn zein composites with strong mechanical properties for adsorption of rare earth elements. J Taiwan Inst Chem Engrs 2018;85:106–14, http://dx.doi.org/10.1016/j.jtice.2017.12.024.
[40] Feng T, Xu J, Yu C, Cheng K, Wu Y, Wang Y, et al. Graphene oxide wrapped melamine sponge as an efficient and recoverable adsorbent for Pb(II) removal from fly ash leachate. J Hazard Mater 2019;367:26–34, http://dx.doi.org/10.1016/j.jhazmat.2018.12.053.
[41] Kamoun EA, Youssef ME, Abu-Saied MA, Fahmy A, Khalil HF, Abdelhai F. Ion conducting nanocomposite membranes based on PVA-HAHAP for fuel cell application: II. Effect of modifier agent of pva on membrane properties. Int J Electrochem Sci 2015;10:6627–44, http://dx.doi.org/10.13140/RG.2.1.2331.6002.
[42] Wang Y, Zheng Y, He W, Wang C, Sun Y, Qiao K, et al. Preparation of a novel sodium alginate/polyvinyl formal composite with a double crosslinking interpenetrating network for multifunctional biomedical application. Composites Part B: Eng 2017;121:9–22, http://dx.doi.org/10.1016/j.compositesb.2017.06.023.
[43] Marcano DC, Kosynkin DV, Berlin JM, Sinitskii A, Sun Z, Slesarev A, et al. Improved synthesis of graphene oxide. ACS Nano 2010;4(8):4806–14, http://dx.doi.org/10.1021/nn1006368.
[44] Anis B, Mostafa A, Sayed ZE, Khalil A, Abouelsayed A. Preparation of highly conductive, transparent, and flexible graphene/silver nanowires substrates using non-thermal laser photoreduction. Opt Laser Technol 2018;103:367–72, http://dx.doi.org/10.1016/j.optlastec.2018.01.057.
[45] Chen T, Zeng B, Liu JL, Dong JH, Liu XQ, Wu Z, et al. High throughput exfoliation of graphene oxide from expanded graphite with assistance of strong oxidant in modified Hummers method. J Phys: Conf Ser 2009;188:012051, http://dx.doi.org/10.1088/1742-6596/188/1/012051.
[46] Pan Y, Wang W, Peng C, Shi K, Luo Y, Ji X. Novel hydrophobic polyvinyl alcohol-formaldehyde foams for organic solvents absorption and effective separation. RSC Adv 2014;4:660–9, http://dx.doi.org/10.1039/C3RA43907K.
[47] Pan Y, Peng C, Wang W, Shi K, Liu Z, Ji X. Preparation and absorption behavior to organic pollutants of macroporous hydrophobic polyvinyl alcohol-formaldehyde sponges. RSC Adv 2014;4:35620–8, http://dx.doi.org/10.1039/C4RA03278K.
[48] Anis B, Abouelsayed A, hotaby WE, Sawy AM, Khalil AS. Tuning the plasmon resonance and work function of laser-scribed chemically doped graphene. Carbon 2017;120:44–53, http://dx.doi.org/10.1016/j.carbon.2017.05.010.
[49] Hsiao ST, Tien HW, Liao WH, Wang YS, Li SM, MMa CC, et al. A highly electrically conductive graphene-silver nanowire hybrid nanomaterial for transparent conductive films. J Mater Chem C 2014;2:7284–91, http://dx.doi.org/10.1039/C4TC01217H.
[50] Lai Q, Zhu S, Luo X, Zou M, Huang S. Ultraviolet-visible spectroscopy of graphene oxides. AIP Adv 2012;2(3):032146, http://dx.doi.org/10.1063/1.4747817.
[51] Malard L, Pimenta M, Dresselhaus G, Dresselhaus M. Raman spectroscopy in graphene. Phys Rep 2009;473(5–6):51–87, doi:https://doi.org/10.1016/j.physrep.2009.02.003.
[52] Ferrari AC, Meyer JC, Scardaci V, Casiraghi C, Lazzeri M, Mauri F, et al. Raman spectrum of graphene and graphene layers. Phys Rev Lett 2006;97:187401, http://dx.doi.org/10.1103/PhysRevLett.97.187401.
[53] Larkin PJ. Illustrated IR and Raman spectra demonstrating important functional groups. In: Larkin PJ, editor. Infrared and Raman spectroscopy. 2nd edition Elsevier; 2018. p. 153–210, http://dx.doi.org/10.1016/B978-0-12-804162-8.00008-2 [chapter 8]. ISBN 978-0-12-804162-8.
[54] Verma S, Dutta RK. A facile method of synthesizing ammonia modified graphene oxide for efficient removal of uranyl ions from aqueous medium. RSC Adv 2015;5:77192–203, http://dx.doi.org/10.1039/C5RA10555B.
[55] Anis B, Fllah HE, Ismail T, Fathallah WM, Khalil A, Hemeda O, et al. Preparation, characterization, and thermal conductivity of polyvinyl-formaldehyde/MWCNTs foam: a low cost heat sink substrate. J Mater Res Technol 2020;9:2934–45, http://dx.doi.org/10.1016/j.jmrt.2020.01.044.
[56] Chakravarty S, Datta A, Sen Sarma N. An electrical solid-state sulphur dioxide vapour sensor based on a polyvinyl alcohol formaldehyde composite. J Mater Chem C 2017;5:2871–82, http://dx.doi.org/10.1039/C7TC00442G.
[57] Xue B, Li R, Deng J, Zhang J. Sound absorption properties of microporous poly(vinyl formal) foams prepared by a two-step acetalization method. Ind Eng Chem Res 2016;55(14):3982–9, http://dx.doi.org/10.1021/acs.iecr.6b00127.
[58] Artyukhov AA, Shtilman MI, Kuskov AN, Pashkova LI, Tsatsakis AM, Rizos AK. Polyvinyl alcohol cross-linked macroporous polymeric hydrogels: structure formation and regularity investigation. J Non-Cryst Solids 2011;357(2):700–6, http://dx.doi.org/10.1016/j.jnoncrysol.2010.06.038.
[59] Zhao B, Hamidinejad M, Zhao C, Li R, Wang S, Kazemi Y, et al. A versatile foaming platform to fabricate polymer/carbon composites with high dielectric permittivity and ultra-low dielectric loss. J Mater Chem A 2019;7:133–40, http://dx.doi.org/10.1039/C8TA05556D.
[60] Ameli A, Jung P, Park C. Electrical properties and electromagnetic interference shielding effectiveness of polypropylene/carbon fiber composite foams. Carbon 2013;60:379–91, http://dx.doi.org/10.1016/j.carbon.2013.04.050.
[61] Zhao G, Li J, Ren X, Chen C, Wang X. Few-layered graphene oxide nanosheets as superior sorbents for heavy metal ion pollution management. Environ Sci Technol 2011;45(24):10454–62, http://dx.doi.org/10.1021/es203439v.
[62] Chowdhury I, Duch MC, Mansukhani ND, Hersam MC, Bouchard D. Colloidal properties and stability of graphene oxide nanomaterials in the aquatic environment. Environ Sci Technol 2013;47(12):6288–96, http://dx.doi.org/10.1021/es400483k.
[63] Kashyap S, Mishra S, Behera SK. Aqueous colloidal stability of graphene oxide and chemically converted graphene. J Nanopart 2014;2014:1–6, http://dx.doi.org/10.1155/2014/640281.

[64] Lotya M, Rakovich A, Donegan JF, Coleman JN. Measuring the lateral size of liquid-exfoliated nanosheets with dynamic light scattering. Nanotechnology 2013;24(26):265703, http://dx.doi.org/10.1088/0957-4484/24/26/265703.
[65] Thomas HR, Day SP, Woodruff WE, Vallés C, Young RJ, Kinloch IA, et al. Deoxygenation of graphene oxide: reduction or cleaning? Chem Mater 2013;25(18):3580–8, http://dx.doi.org/10.1021/cm401922.
[66] Rao MM, Ramana D, Seshaiah K, Wang M, Chien SC. Removal of some metal ions by activated carbon prepared from Phaseolus aureus hulls. J Hazard Mater 2009;166(2):1006–13, http://dx.doi.org/10.1016/j.jhazmat.2008.12.002.
[67] Moharram MAK, Tohami K, Hotaby WME, Bakr AM. Graphene oxide porous crosslinked cellulose nanocomposite microspheres for lead removal: kinetic study. React Funct Polym 2016;101:9–19, http://dx.doi.org/10.1016/j.reactfunctpolym.2016.02.001.
[68] Aydın H, Bulut Y, Yerlikaya C. Removal of copper (II) from aqueous solution by adsorption onto low-cost adsorbents. J Environ Manag 2008;87(1):37–45, http://dx.doi.org/10.1016/j.jenvman.2007.01.005.
[69] Kannan N, Veemaraj T. Removal of lead(II) ions by adsorption onto bamboo dust and commercial activated carbons – a comparative study. E-J Chem 2009;6(1):247–56, http://dx.doi.org/10.1155/2009/515178.
[70] Dehghani MH, Taher MM, Bajpai AK, Heibati B, Tyagi I, Asif M, et al. Removal of noxious Cr (VI) ions using single-walled carbon nanotubes and multi-walled carbon nanotubes. Chem Eng J 2015;279:344–52, http://dx.doi.org/10.1016/j.cej.2015.04.151.
[71] Rao MM, Rao GC, Seshaiah K, Choudary N, Wang M. Activated carbon from Ceiba pentandra hulls, an agricultural waste, as an adsorbent in the removal of lead and zinc from aqueous solutions. Waste Manag 2008;28(5):849–58, http://dx.doi.org/10.1016/j.wasman.2007.01.017.
[72] Ho Y, McKay G. A comparison of chemisorption kinetic models applied to pollutant removal on various sorbents. Process Saf Environ Protect 1998;76(4):332–40, http://dx.doi.org/10.1205/095758298529696.
[73] Yu F, Wu Y, Ma J, Zhang C. Adsorption of lead on multi-walled carbon nanotubes with different outer diameters and oxygen contents: kinetics, isotherms and thermodynamics. J Environ Sci 2013;25(1):195–203, http://dx.doi.org/10.1016/S1001-0742(12)60023-0.
[74] Weber WJ, Morris JC. Kinetics of adsorption on carbon from solution. J Sanit Eng Div 1963;89:31–60 https://cedb.asce.org/CEDBsearch/record.jsp?dockey=0013042.
[75] Mckay G, Allen SJ. Surface mass transfer processes using peat as an adsorbent for dyestuffs. Can J Chem Eng 1980;58(4):521–6, http://dx.doi.org/10.1002/cjce.5450580416.
[76] Langmuir I. The constitution and fundamental properties of solids and liquids. Part I. Solids. J Am Chem Soc 1916;38(11):2221–95, http://dx.doi.org/10.1021/ja02268a002.
[77] Schiewer S, Patil SB. Pectin-rich fruit wastes as biosorbents for heavy metal removal: equilibrium and kinetics. Bioresour Technol 2008;99(6):1896–903, http://dx.doi.org/10.1016/j.biortech.2007.03.060.
[78] Gunay A, Arslankaya E, Tosun I. Lead removal from aqueous solution by natural and pretreated clinoptilolite: adsorption equilibrium and kinetics. J Hazard Mater 2007;146(1):362–71, http://dx.doi.org/10.1016/j.jhazmat.2006.12.034.
[79] Mobasherpour I, Salahi E, Ebrahimi M. Thermodynamics and kinetics of adsorption of Cu(II) from aqueous solutions onto multi-walled carbon nanotubes. J Saudi Chem Soc 2014;18(6):792–801, http://dx.doi.org/10.1016/j.jscs.2011.09.006.
[80] Wang CC, Juang LC, Lee CK, Hsu TC, Lee JF, Chao HP. Effects of exchanged surfactant cations on the pore structure and adsorption characteristics of montmorillonite. J Colloid Interface Sci 2004;280(1):27–35, http://dx.doi.org/10.1016/j.jcis.2004.07.009.
[81] Li YH, Ding J, Luan Z, Di Z, Zhu Y, Xu C, et al. Competitive adsorption of Pb^{2+}, Cu^{2+} and Cd^{2+} ions from aqueous solutions by multiwalled carbon nanotubes. Carbon 2003;41(14):2787–92, http://dx.doi.org/10.1016/S0008-6223(03)00392-0.
[82] Awual MR. Innovative composite material for efficient and highly selective Pb(II) ion capturing from wastewater. J Mol Liq 2019;284:502–10, http://dx.doi.org/10.1016/j.molliq.2019.03.157.
[83] Awual MR, Islam A, Hasan MM, Rahman MM, Asiri AM, Khaleque MA, et al. Introducing an alternate conjugated material for enhanced lead(II) capturing from wastewater. J Clean Prod 2019;224:920–9, http://dx.doi.org/10.1016/j.jclepro.2019.03.241.
[84] Awual MR, Hasan MM, Islam A, Rahman MM, Asiri AM, Khaleque MA, et al. Offering an innovative composited material for effective lead(II) monitoring and removal from polluted water. J Clean Prod 2019;231:214–23, http://dx.doi.org/10.1016/j.jclepro.2019.05.125.